Multiple Substitution Strategies toward Tunable Luminescence in Lu$_2$MgAl$_4$SiO$_{12}$:Eu^{2+} Phosphors

Zhiqiang Ming,[†] Jianwei Qiao,[†] Maxim S. Molokeev,[‡,§,⊥] Jing Zhao,[†] Hendrik C. Swart,[△] and Zhiguo Xia*,[†,◇]

[†]School of Materials Sciences and Engineering, University of Science and Technology Beijing, Beijing 100083, China

[‡]Laboratory of Crystal Physics, Kirensky Institute of Physics, Federal Research Center Krasnoyarsk Scientific Center of the Siberian Branch of the Russian Academy of Sciences, Krasnoyarsk 660036, Russia

[§]Siberian Federal University, Krasnoyarsk, 660041, Russia

[⊥]Department of Physics, Far Eastern State Transport University, Khabarovsk 680021, Russia

[△]Department of Physics, University of the Free State, P.O. Box 339, Bloemfontein 9300, South Africa

[◇]State Key Laboratory of Luminescent Materials and Devices and Institute of Optical Communication Materials, South China University of Technology, Guangzhou 510641, China

ⓈSupporting Information

ABSTRACT: The equivalent or heterovalent substitution strategy is an efficient way to stimulate photoluminescence tuning or to optimize the luminescence performances of phosphor materials. Garnet-type compounds receive much attention as phosphor hosts because of their flexible structural frameworks. Herein, a garnet-type Lu$_2$MgAl$_4$SiO$_{12}$:Eu^{2+} phosphor with broad-band blue-green emission is first explored with two-site occupation by varying the Eu^{2+} content. Two host-substitution approaches to controlling the luminescence behavior of Lu$_2$MgAl$_4$SiO$_{12}$:Eu^{2+} phosphor are implemented. The cation substitution strategy of Ca^{2+} for Mg^{2+} achieves tunable emission from 463 to 503 nm together with broadening emission bands in Lu$_2$Mg$_{1−y}$Ca$_y$Al$_4$SiO$_{12}$:Eu^{2+} phosphors. Moreover, chemical unit cosubstitution of [Ca^{2+}−Ge^{4+}] replacing [Lu^{3+}−Al^{3+}] results in Lu$_{2−z}$Ca$_z$MgAl$_{4−z}$Ge$_z$SiO$_{12}$:Eu^{2+} phosphors, which induce a red shift of the emission peak of about 60 nm and a broadening in the emission spectra with increasing Ca^{2+} and Ge^{4+} concentrations. The possible photoluminescence tuning mechanism is ascribed to the coordination sphere variation in the EuO$_8$ polyhedron depending on the changing neighboring cations. The proposed approaches on equivalent or heterovalent substitution can contribute to the development of Eu^{2+}-activated garnet-type phosphors with regulation of the luminescence performance and further initiate research discovering new phosphors for white-light-emitting diodes.
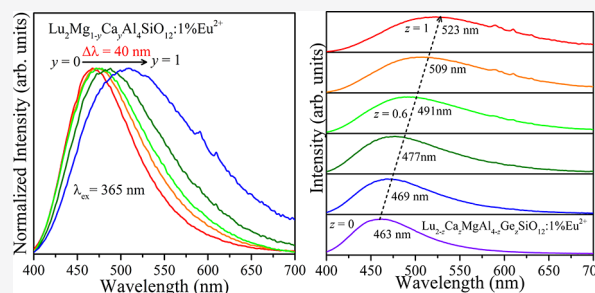
INTRODUCTION

Phosphor-converted white-light-emitting diodes (w-LEDs) have received growing attention because of their superior performance such as low energy consumption, wide color tunability, and long duration time.[1,2] To obtain ideal w-LEDs, it is essential to improve the characteristic photoluminescence (PL) properties of phosphor materials because the phosphor materials used significantly affect the performance of w-LEDs, especially the color rendition and luminous efficiency.[3−5] To date, many important phosphor hosts are built upon the existing structural models, and some typical ones include the garnet-type, Si$_3$N$_4$-type, apatite-type, melilite-type, A$_3$MX$_5$-type, UCr$_4$C$_4$-type, and β-K$_2$SO$_4$-type models, and so on.[5−11] Among the various structure models, garnet-type compounds with cubic structure have been widely utilized as hosts to be applied in illumination and display fields. The garnet host possesses the general formula A$_3$B$_2$C$_3$O$_{12}$ with three different cation sites that give more flexible compositions by altering the substitution of A, B, and C cations.[6] Moreover, the extensive concern about garnet-type phosphors puts Ce^{3+} as a luminous center because of the excellent luminescence properties with broadband excitation in the ultraviolet (UV) or blue-light region.[12] For instance, the excitation spectrum of a commercial Lu$_3$Al$_5$O$_{12}$:Ce^{3+} phosphor can match well with the emission of a blue LED chip, and one can further easily obtain tunable luminescence in Lu$_3$Al$_5$O$_{12}$:Ce^{3+} by changing the chemical compositions.[13] Eu^{2+} acts as the same important activator as Ce^{3+}, while there is rare research about the garnet-type phosphor with Eu^{2+} as the activator, which is ascribed to the fact that most garnet-type hosts do not have a suitable coordination environment for Eu^{2+} occupation. Chen et al. recently reported a blue-emitting phosphor, Lu$_2$CaMg$_2$Si$_3$O$_{12}$:Eu^{2+}, and no obvious Eu^{3+} emission exists

under 365 nm excitation.[14] $Y_2Mg_2Al_2Si_2O_{12}$:Eu^{2+} with a tunable emission peak from 436 to 491 nm was reported by Zhang et al.[15] Besides, the Eu^{2+}-doped $Ca_3Sc_2Si_3O_{12}$ phosphor exhibits surprising near-IR emission under 520 nm excitation.[16] It is worthwhile to study a Eu^{2+}-doped garnet-type phosphor because it will lead to an unexpected luminescence and potential applications.

To obtain optimized luminescence properties, including the positions of the excitation and emission along with the spectral bandwidth, the solid solution design based on the equivalent or heterovalent substitution strategy acts as one of the most efficient approaches.[4,17] The ordinarily used design principles mainly contain the cation/anion substitution, cation-pair substitution, and chemical unit cosubstitution.[18,19] For example, the red-shift phenomenon was observed in the $Ca_9Y(PO_4)_7$:Eu^{2+} phosphor when the Sr^{2+}-substituted Ca^{2+} and Mg^{2+}-substituted Ca^{2+} and the positions of the emission peaks moved toward shorter wavelengths.[20] Liang et al. reported the color-tunable emission in $Sr_3Al_{2-x}Si_xO_{5-x}N_xCl_2$:$Eu^{2+}$ by means of cosubstituting Al^{3+}−O^{2-} with Si^{4+}−N^{3-}.[21] Our group also reported the tunable emission in $Ca_9MgK(PO_4)_7$:Eu^{2+} via cation substitution with an adjustable chemical environment, and, more importantly, our group first summarized the concept of chemical unit cosubstitution with the example of $Ca_2(Al_{1-x}Mg_x)(Al_{1-x}Si_{1+x})O_7$:$Eu^{2+}$ phosphors.[22,23]

In this work, Eu^{2+}-doped $Lu_2MgAl_4SiO_{12}$ phosphors were first prepared. The proposed solid solution strategies including cation substitution and chemical unit cosubstitution have been used to realize tunable emission in this system. Besides, the correlation of the crystal structure and luminescence properties of the garnet-type phosphor was investigated in detail. To obtain tunable and optimized luminescence properties, the substitution of Ca^{2+} ions for Mg^{2+} ions in the $Lu_2MgAl_4SiO_{12}$:Eu^{2+} systems was designed, and its influence on the luminescence and possible red-shift mechanisms were studied. Moreover, the [Ca^{2+}−Ge^{4+}] unit was also introduced to the $Lu_2MgAl_4SiO_{12}$:Eu^{2+} systems to achieve adjustment of the emission spectra. Commonly, tunable luminescence can be achieved efficiently in Eu^{2+}-activated garnet-type phosphors, which serves a guide in the development of novel Eu^{2+}-doped garnet-type phosphors for w-LEDs.

■ EXPERIMENTAL SECTION

Materials and Preparation. $Lu_2MgAl_4SiO_{12}$:xEu^{2+}, $Lu_2Mg_{1-y}Ca_yAl_4SiO_{12}$:$1\%Eu^{2+}$, and $Lu_{2-z}Ca_zMgAl_{4-z}Ge_zSiO_{12}$:$1\%$ Eu^{2+} powders were prepared by the solid-state reaction method. Lu_2O_3 (99.99%), MgO (analytical reagant, A.R.), Al_2O_3 (A.R.), SiO_2 (A.R.), $CaCO_3$ (A.R.), GeO_2 (A.R.), and Eu_2O_3 (99.99%) were used as raw materials, and 3 wt % H_3BO_3 (99.99%) was added as the flux. Stoichiometric amounts of the starting materials were weighed and then ground together with ethanol as the dispersing agent using an agate mortar and pestle until the mixtures were almost dry (30 min). Then the powder mixtures were sintered at 1400 °C for 4 h in a tube furnace under a reducing atmosphere of N_2−H_2 (20%). After firing, the samples were cooled to room temperature in the furnace and ground again for further characterization.

Characterization. The powder diffraction (XRD) patterns of the samples were measured by using a D8 Advance diffractometer (Bruker Corp., Germany) with monochromatized Cu $K\alpha$ radiation (λ = 1.5406 Å) for crystal structure and phase analysis. Also, the testing environment of the instrument was operating at room temperature with 40 kV and 40 mA. The step scanning range of 2θ was from 5° to 120° for Rietveld refinements. The step width of 2θ was 0.013° with a scanning speed of 2 s of counting time per step. Rietveld structure

refinements were conducted by using *TOPAS 4.2* software. The room temperature photoluminescence excitation (PLE) and PL spectra were measured by using a FLS920 fluorescence spectrophotometer (Edinburgh Instruments Ltd., U.K.). The luminescence decay curves were also collected by a FLS920 instrument at room temperature and excited by a nF900 flash lamp. The PL quantum efficiency was measured at room temperature by using an absolute quantum efficiency measurement system (C9920-02, Hamamatsu Photonics) with an integrating sphere.

■ RESULTS AND DISCUSSION

Phase Identification and Crystal Structure Analysis. The XRD patterns of the as-prepared $Lu_2MgAl_4SiO_{12}$:xEu^{2+}, $Lu_2Mg_{1-y}Ca_yAl_4SiO_{12}$:$1\%$ Eu^{2+}, and $Lu_{2-z}Ca_zMgAl_{4-z}Ge_zSiO_{12}$:$1\%Eu^{2+}$ samples are shown in Figure 1. Obviously, the XRD patterns of these samples are in good agreement with the standard card (PDF 73-1368) pattern of $Lu_3Al_5O_{12}$ from Figure 1a, suggesting that the doping of Eu^{2+} does not influence the phase purity and Eu^{2+} ions are doped in the host lattice. It is noticed that the XRD peaks of the enlarged XRD patterns systematically shift toward lower angles, as seen for the peak position of the (211) plane when x increased, indicating a lattice expansion due to replacement of the small Lu^{3+} (CN = 8 and R = 0.977 Å, where CN stands for the coordination number and R the ionic radius, hereafter) and Mg^{2+} (CN = 8 and R = 0.89 Å) with the big Eu^{2+} (CN = 8 and R = 1.25 Å). In addition, Rietveld refinement was performed by using *TOPAS 4.2* for the $Lu_2MgAl_4SiO_{12}$:$1\%Eu^{2+}$ samples. The cell parameters were $a = b = c$ = 11.8574(1) Å, and the cell volume is 1667.14(4) Å. According to the refinement result from Figure 2a, almost all of the peaks of the studied samples were indexed to a cubic cell ($Ia\bar{3}d$) with parameters close to $Lu_3Al_5O_{12}$ besides small impurity peaks of the Mg_2SiO_4 phase. On the basis of the previous papers, the trace impurity Mg_2SiO_4 has no effect on the luminescence of $Lu_2MgAl_4SiO_{12}$:xEu^{2+} because Eu-doped Mg_2SiO_4 cannot retain the divalent state and show emission.[24] The results of Rietveld refinement displayed that Eu^{2+} occupied the crystallographic sites of Lu^{3+} and Mg^{2+}. The detailed information on the main parameters of processing and refinement, fractional atomic coordinates and isotropic displacement parameters (Å^2), and main bond lengths (Å) of the $Lu_2MAl_4SiO_{12}$:$1\%Eu^{2+}$ (M = Ca, Mg) samples are given in Tables S1−S3, respectively.

The XRD patterns of $Lu_2Mg_{1-y}Ca_yAl_4SiO_{12}$:$1\%Eu^{2+}$ matched well with the standard card pattern of $Lu_3Al_5O_{12}$ from Figure 1b, indicating that the replacement of Ca^{2+} with Mg^{2+} has no influence on the crystal structure. Because the big-ionic-radius Ca^{2+} substitutes for the small-ionic-radius Mg^{2+}, causing lattice expansion, enlarged XRD patterns show a simultaneous shift toward lower angles in the peak position of the (211) plane with Ca^{2+} doping. The result of Rietveld refinement shown in Figure 2b shows that the phase of the as-prepared sample $Lu_2CaAl_4SiO_{12}$:$1\%Eu^{2+}$ is pure. Figure 1c presents the XRD patterns of the products with Ca^{2+}−Ge^{4+} codoping in the $Lu_2MgAl_4SiO_{12}$:$1\%Eu^{2+}$ system. All of the diffraction peaks of the samples with [Ca^{2+}−Ge^{4+}] codoping can be ascribed to a pure cubic $Lu_3Al_5O_{12}$ phase, and the diffraction peak of the (211) plane also gradually shifted to lower angles with the doping of Ca and Ge ions, which proved the successful doping of the [Ca^{2+}−Ge^{4+}] unit cosubstitution process.

Figure 3 summarizes the different crystal structure evolution routes from the $Lu_2MgAl_4SiO_{12}$ matrix to the
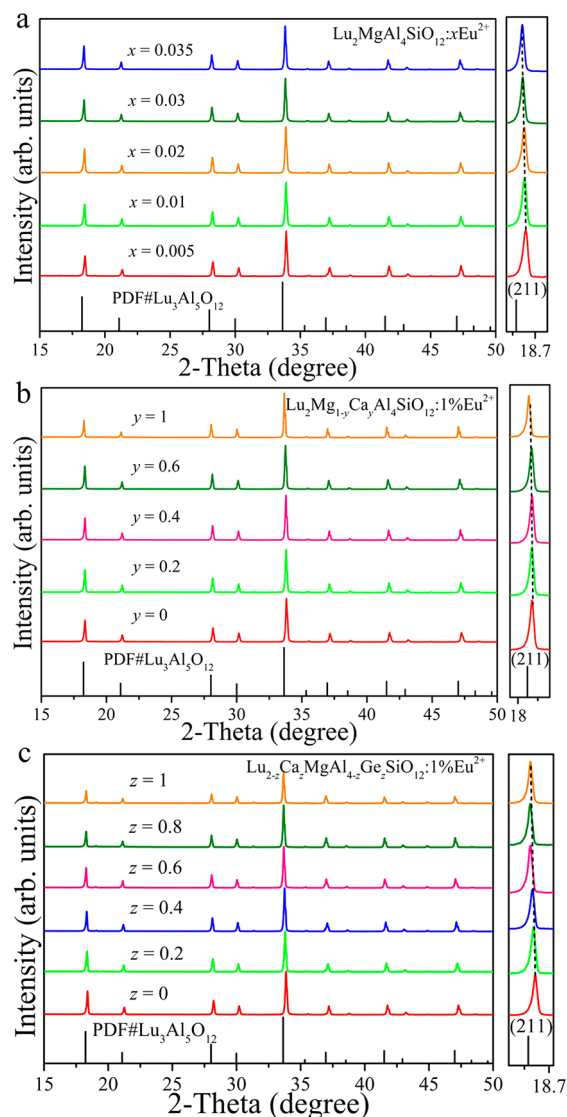
Figure 1. (a) XRD patterns of the $Lu_2MgAl_4SiO_{12}:xEu^{2+}$ powders with $x = 0.005-0.035$. Enlarged XRD patterns show a systematic shift in the peak position of the (211) plane with Eu^{2+} doping. (b) XRD patterns of the $Lu_2Mg_{1-y}Ca_yAl_4SiO_{12}:1\%Eu^{2+}$ powders with $y = 0-1$. Enlarged XRD patterns show a systematic shift at the peak position of the (211) plane with Ca^{2+} doping. (c) XRD patterns of the $Lu_{2-z}Ca_zMgAl_{4-z}SiGe_zO_{12}:1\%Eu^{2+}$ powders with $z = 0-1$. Enlarged XRD patterns show a systematic shift in the peak position of the (211) plane with $Ca^{2+}-Ge^{4+}$ codoping.

$Lu_2MgAl_4SiO_{12}:1\%Eu^{2+}$, $Lu_2CaAl_4SiO_{12}:1\%Eu^{2+}$, and $LuCaMgAl_3GeSiO_{12}:1\%Eu^{2+}$ phosphors via the substitution strategy. Apparently, some ions occupy the octahedral site, Al2 and Si form the $Al2/SiO_4$ tetrahedron, and Lu and Mg occupy the interstitial site of $Al1O_6$, connecting with $Al2/SiO_4$ by corner-sharing. With Ca^{2+} or $[Ca^{2+}-Ge^{4+}]$ doping, the coordination environment of Eu^{2+} changed, which may cause variation of the luminescent properties.

PL Properties of $Lu_2MgAl_4SiO_{12}:Eu^{2+}$. The room temperature excitation and emission spectra of $Lu_2MgAl_4SiO_{12}$ doped with 1% Eu^{2+} are shown in Figure 4a, along with the inset actual photograph of the sample under 365 nm UV-lamp irradiation. The $Lu_2MgAl_4SiO_{12}:1\%Eu^{2+}$ phosphor exhibited a broad excitation band covering a spectral range of 250−450 nm, which means that it can match well with the n-UV LED
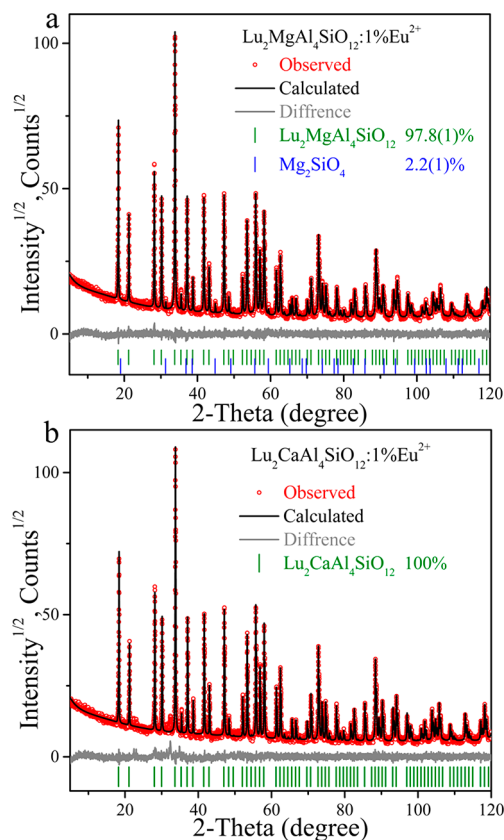
Figure 2. Rietveld refinement XRD patterns of (a) $Lu_2MgAl_4SiO_{12}:1\%Eu^{2+}$ and (b) $Lu_2CaAl_4SiO_{12}:1\%Eu^{2+}$.

chips, which is attributed to the electronic transitions of Eu^{2+} from its 4f ground state to the field-splitting levels of its 5d state. The PL spectrum of $Lu_2MgAl_4SiO_{12}:1\%Eu^{2+}$ consisted of one broad nonsymmetrical band with a peak at about 463 nm under an excitation of 365 nm UV radiation and a tail at the long-wavelength side, indicating that at least two emission centers exist. The broad emission band can be deconvoluted into two sub-Gaussian components, suggesting the different occupancies of Eu^{2+}, peaking at ∼454 nm (22026 cm^{-1}) and ∼500 nm (20000 cm^{-1}), as shown in Figure 4b.

To further know the origin of the luminescence center Eu^{2+} in the $Lu_2MgAl_4SiO_{12}$ phosphor, the empirical Van Uitert equation was used to analyze the results of the emission spectra. The equation is given as follows according to a previous report:[25,26]

$$E = Q\left[1 - \left(\frac{V}{4}\right)^{1/V} \times 10^{-nE_a r/80}\right] \tag{1}$$

where E is the position of the Eu^{2+} emission peak (cm^{-1}), Q is the position in energy for the lower d-band edge of the free Eu^{2+} ion (34 000 cm^{-1} for Eu^{2+}), V is the valence of the Eu^{2+} ion (the V value is 2), n is the number of anions in the immediate shell about the Eu^{2+} ion, E_a is the electron affinity of the atoms of the anions (it is a constant for the same host), r is the radius of the cation replaced by the Eu^{2+} ion (Å).[15,27] The coordination number of both Lu and Mg is 8 in the Eu^{2+}-doped $Lu_2MgAl_4SiO_{12}$ phosphor. On the basis of the above analysis, it is obvious that E is proportional to r. Considering that the radius of Lu is larger than that of Mg in $Lu_2MgAl_4SiO_{12}$, the emission band peaking at 454 nm belongs
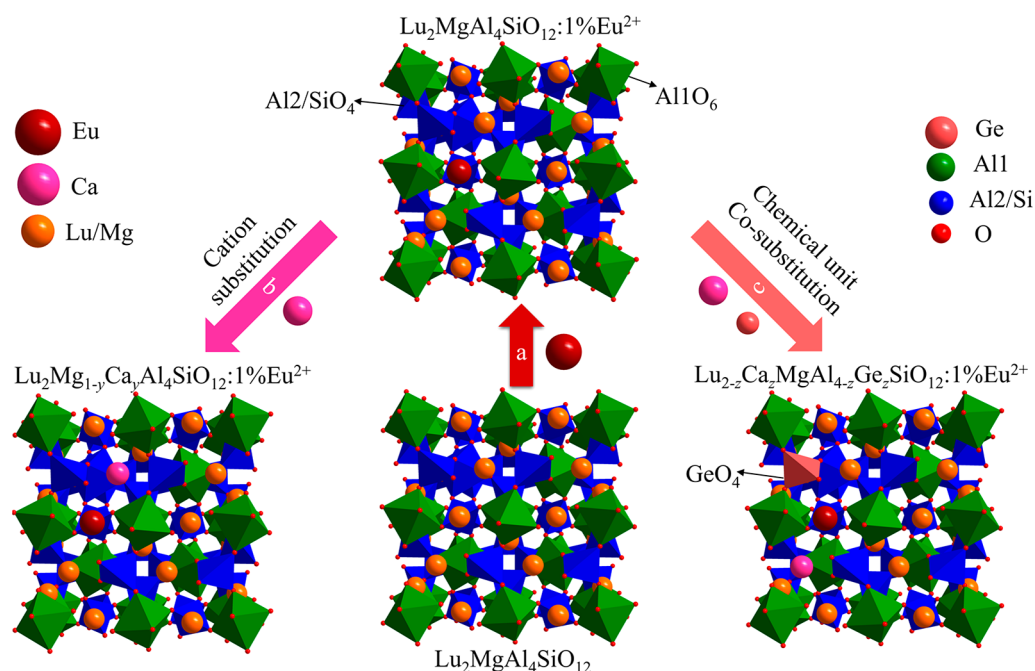
Figure 3. Crystal structure evolution (a) from the $Lu_2MgAl_4SiO_{12}$ matrix to $Lu_2MgAl_4SiO_{12}$:1%Eu^{2+} by doping Eu^{2+} ions, (b) $Lu_2Mg_{1−y}Ca_yAl_4SiO_{12}$:1%$Eu^{2+}$ by cation substitution of Mg^{2+} with a bigger cation Ca^{2+}, and (c) $Lu_{2−z}Ca_zMgAl_{4−z}SiGe_zO_{12}$:1%$Eu^{2+}$ by chemical unit cosubstitution of [$Lu^{3+}−Al^{3+}$] with [$Ca^{2+}−Ge^{4+}$].

to Eu^{2+} occupying the Lu site and the emission band peaking at 500 nm is ascribed to that of Eu^{2+} occupying the Mg site. The measured emission spectra have emission peaks centered at 463 nm near 454 nm, which can draw a conclusion that Eu^{2+} preferentially occupies the 8-fold-coordinated Lu sites in the $Lu_2MgAl_4SiO_{12}$ structure. Figure 4c shows the decay curves of $Lu_2MgAl_4SiO_{12}$:1%Eu^{2+} at room temperature monitored under excitation at 365 nm and emission at 463 nm. This fluorescence decay curve can be well-fitted by the second-order exponential function[25]

$$I(t) = A_1 \exp(-t/\tau_1) + A_2 \exp(-t/\tau_2) \qquad (2)$$

where $I(t)$ is the luminescence intensity, A_1 and A_2 are constants, t is time, and τ_1 and τ_2 are the lifetimes for the exponential components. Furthermore, the average decay time value (τ_{av}) was calculated using the following equation:[20]

$$\tau_{av} = (A_1\tau_1^{\,2} + A_2\tau_2^{\,2})/(A_1\tau_1 + A_2\tau_2) \qquad (3)$$

Upon calculation, the average lifetime is determined as 0.881 μs, and the second-order exponential behavior also verifies the existence of two different emission centers. Under 365 nm excitation, the PL spectra of the samples $Lu_2MgAl_4SiO_{12}$:$x$$Eu^{2+}$, with x changing from 0.5% to 3.5%, are depicted in Figure 5a. Obviously, the emission intensity of the samples reaches its maximum when x is 1%, and then the concentration quenching effect results in a decline of the emission intensity. The concentration quenching effect is caused by excitation energy transfer among Eu^{2+} ions at higher concentration. According to the formula of Blasse,[26] the calculated critical distance between the Eu^{2+} ions in the $Lu_2MgAl_4SiO_{12}$:$x$$Eu^{2+}$ system is 34.0 Å, indicating that the electric multipolar interactions govern the energy transfer among Eu^{2+} ions. The relationship between the PL intensity and concentration of Eu^{2+} is as shown in Figure S1 by using the Dexter theory analysis, and the concentration quenching

mechanism of Eu^{2+} is ascribed to the electric dipole−dipole interactions. The quantum efficiency of the selected $Lu_2MgAl_4SiO_{12}$:1%Eu^{2+} phosphor excited at 365 nm is 39.36%, as shown in Table S4, and the values of other samples are also listed. From the normalized PL spectra of the $Lu_2MgAl_4SiO_{12}$:$x$$Eu^{2+}$ phosphors, as displayed in Figure 5b, a 15 nm red shift of the emission peak position was observed, meaning the possibility of a spectral peak regulated by control of the Eu^{2+} concentration, which may be attributed to an increase in the crystal-field splitting. Meanwhile, the inset shows the CIE chromaticity coordinates of the phosphors from the blue region shifting toward the blue-green region with increasing x, as shown in Figure 5b.

PL Tuning via Cation Substitution. By means of cation substitution in the $Lu_2MgAl_4SiO_{12}$:1%Eu^{2+} phosphor, the emission color of the phosphors can be tuned by changing the crystal-field environment of the doped activators. $Lu_2MgAl_4SiO_{12}$ is isotypic to $Lu_2CaAl_4SiO_{12}$, and therefore it can form a complete solid solution by cation substitution because of the small gap in the ion radius between the Ca^{2+} and Mg^{2+}. The normalized emission spectra of the phosphors $Lu_2Mg_{1−y}Ca_yAl_4SiO_{12}$:1%$Eu^{2+}$ are given in Figure 6a under monitoring at 365 nm, and the value of y in the solid solution was varied from 0 to 1. The emission peak shape and position vary with the Ca^{2+} concentration. The change of the emission peak shape may come from part of the Eu^{2+} ion at the position of the Ca^{2+} site. The sample with $y = 0$ exhibits a wide asymmetric emission band with one peak at 463 nm without any characteristic emission of Eu^{3+}. However, the broadband emission peak shifts to longer wavelength and reaches 488 nm as $y = 0.6$. Simultaneously, the emission spectra of the $y = 0.6$ sample appear at the emission peaks of 591 and 612 nm belonging to Eu^{3+}, indicating that the crystal structure rigidity of the Eu^{2+} local coordination environment may decrease at higher Ca^{2+} content. The decrease of the crystal structure rigidity would lead to an oxidation process from Eu^{2+} to Eu^{3+}

Figure 4. (a) PLE and PL spectra of the $Lu_2MgAl_4SiO_{12}$:1%Eu^{2+} phosphors monitored at room temperature. The inset shows the phosphor images under 365 nm UV light. (b) Gaussian fitting results of PL bands for $Lu_2MgAl_4SiO_{12}$:1%Eu^{2+}. (c) Decay curves of $Lu_2MgAl_4SiO_{12}$:1%Eu^{2+} measured at room temperature with an emission wavelength at 463 nm and an excitation wavelength at 365 nm.

Figure 5. (a) PL spectra of the $Lu_2MgAl_4SiO_{12}$:$x$$Eu^{2+}$ phosphors monitored at 365 nm. The inset shows the PL maximum intensity of $Lu_2MgAl_4SiO_{12}$:$x$$Eu^{2+}$. (b) Normalized PL spectra of the $Lu_2MgAl_4SiO_{12}$:$x$$Eu^{2+}$ phosphors monitored at 365 nm. The inset shows the CIE chromaticity coordinates.
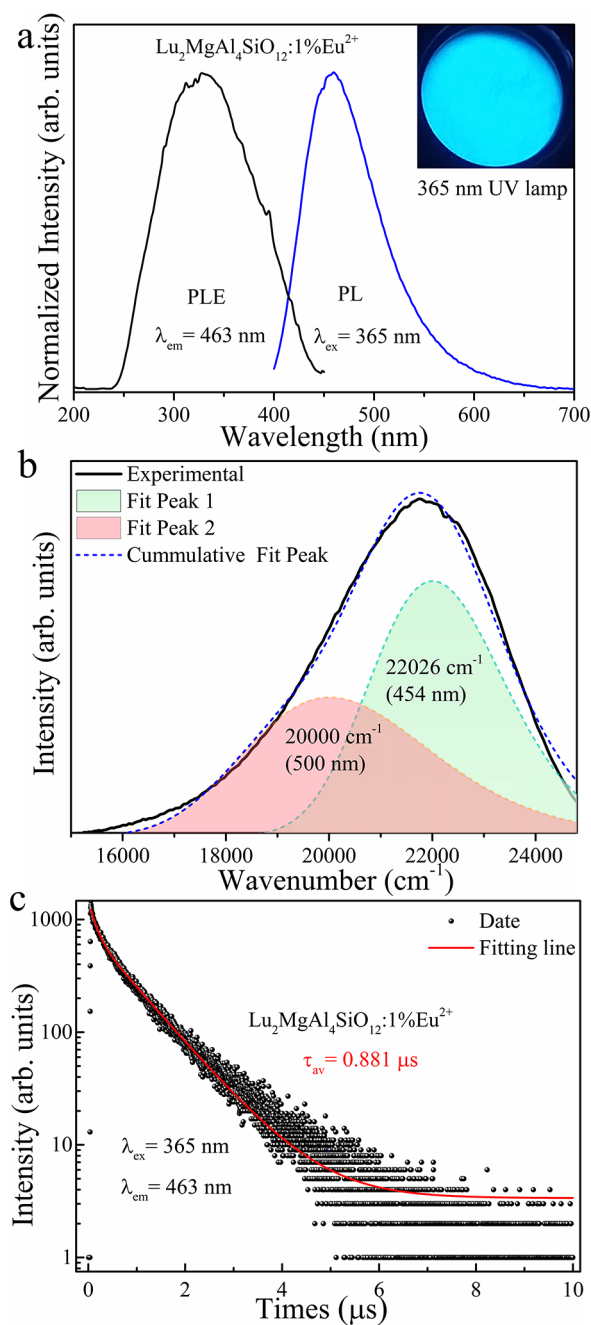
because the Eu^{2+} ions that occupy the Lu^{3+} sites may more easily react with O and become trivalent. The emission peak gradually red-shifted with an increase in the y value, eventually reaching 503 nm when the Ca^{2+} ion absolutely replaced the Mg^{2+} ion ($y = 1$).

As shown in the inset of Figure 6b, the CIE chromaticity coordinates of the $Lu_2Mg_{1-y}Ca_yAl_4SiO_{12}$:1%$Eu^{2+}$ samples shift from (0.174, 0.198) toward (0.299, 0.394) with an increase in the amount of y. The Stokes shift leads to a great difference in the position of the emission peak, so an increase of the Stokes

shift could explain the red-shift phenomenon of the emission spectra. Correspondingly, the Stokes shifts obtained by considering the difference between the emission and excitation spectra and the full width at half-maximum (fwhm) values of the emission spectra are displayed in Figure 6b. Overall, the Stokes shifts of the $Lu_2Mg_{1-y}Ca_yAl_4SiO_{12}$:1%$Eu^{2+}$ phosphors increase, with the y value increasing from 0 to 1, which agrees well with the red-shift phenomenon. Meanwhile, an increase of the Ca^{2+} content also leads to a broadening of the emission bands of the $Lu_2Mg_{1-y}Ca_yAl_4SiO_{12}$:1%$Eu^{2+}$ phosphors, as displayed in Figure 6b, which is propitious to improving the color-rendering index. The crystal-field splitting of the Eu^{2+} 5d levels can also affect the emission peak shift, affecting the position of the lowest 5d levels. Also, the crystal-field-splitting energy is based on the following equation:[25,28,29]

$$D_q = \frac{ze^2r^4}{6R^5} \tag{4}$$

In the above equation, D_q is the crystal-field-splitting energy, R represents the distance between the central ion Eu^{2+} and its ligands, z represents the anion charge, e is the charge of the electron, and r is the radius of the d wave function. If the value of D_q is smaller, the emission peak will locate at the higher-energy direction. Contrarily, the larger value of D_q causes the
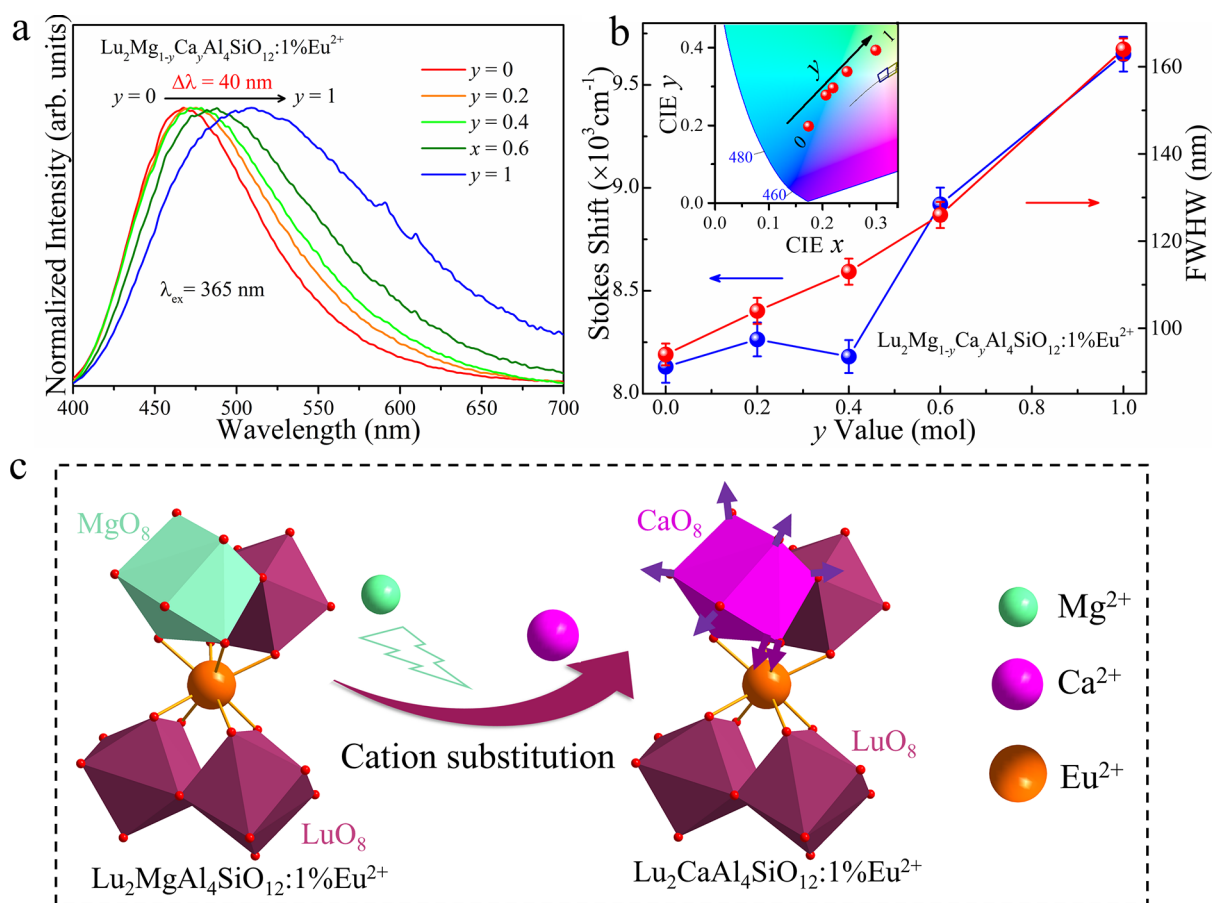
Figure 6. (a) Normalized PL spectra of the $Lu_2Mg_{1-y}Ca_yAl_4SiO_{12}:1\%Eu^{2+}$ phosphors monitored at 365 nm. (b) Stokes shift and fwhm values of the $Lu_2Mg_{1-y}Ca_yAl_4SiO_{12}:1\%Eu^{2+}$ phosphors. The inset shows the CIE chromaticity coordinates. (c) Shrinkage mechanism of the EuO_8 polyhedron with Ca^{2+} substituted for Mg^{2+} in $Lu_2Mg_{1-y}Ca_yAl_4SiO_{12}:1\%Eu^{2+}$.

emission peak to locate at the lower-energy direction.[29] According to the refinement results, the bond length of Lu/Mg/Eu−O in the $y = 0$ sample is smaller than that of Lu/Ca/Eu−O in the $y = 1$ sample, indicating that Ca^{2+} replacement of Mg^{2+} may expand the average Eu−O bond length. Considering that Z, e, and r remain constant in the same host, the crystal-field-splitting energy will decrease with increasing amounts of Ca^{2+}, causing a blue shift of the emission, which contradicts with the experimental results of the emission spectra that red-shifted, as shown in Figure 6a.

Apart from the Eu−O bond length, the crystal-field strength is also dependent on the local symmetry of the Eu^{2+} sites. In addition, the substitution of Mg^{2+} for Ca^{2+} would change the symmetry of the $Lu_2MgAl_4SiO_{12}:1\%Eu^{2+}$ crystal structure, which may strengthen or weaken the crystal-field splitting of the Eu^{2+} 5d levels. The polyhedral distortion index (D) influences the symmetry of the crystal structure, and it can be calculated by[27,30,31]

$$D = \frac{1}{n}\sum_{i=1}^{n}\frac{|l_i - l_{av}|}{l_{av}} \qquad (5)$$

where l_i is the distance from the central atom Eu to the ith coordinating atom and l_{av} is the average bond length. On the basis of the data of the Eu^{2+}−O^{2-} bond length from the refinement results, the polyhedral distortion index of the EuO_8 polyhedron enlarged from $D = 2.38\%$ to $D = 2.88\%$ along with Ca^{2+} replacement of Mg^{2+}, also decreasing the lattice symmetry

of the Eu^{2+} sites. As a result, the emission band broadened and the emission peaks generated a red shift in the $Lu_2Mg_{1-y}Ca_yAl_4SiO_{12}:1\%Eu^{2+}$ system. Previous work has displayed that the bigger the polyhedral distortion index, the bigger the crystal-field splitting.[9,30] Hence, degradation of the lattice symmetry of the Eu^{2+} sites may provide a more substantial contribution to enhancement of the crystal-field splitting than the distance between the Eu^{2+} and O^{2-} ions in this system, which consequently brought about a red shift of the emission spectrum. From the point of the local coordination environment around the Eu^{2+} ion in this compound, the EuO_8 polyhedron has joint edges with the $(Lu/Mg)O_8$ polyhedron; the systematic model exhibits shrinkage of the EuO_8 polyhedron with deterioration in the structure symmetry of the Eu dodecahedron due to the bigger CaO_8 polyhedron substituting for the smaller MgO_8 polyhedron in the second sphere, as illustrated in Figure 6c. Consequently, emission spectra were simultaneously broadened and red-shifted following an increase of the y value.

PL Tuning via Chemical Unit Cosubstitution. As another PL tuning strategy for the $Lu_2MgAl_4SiO_{12}:1\%Eu^{2+}$ sample, the chemical unit cosubstitution of $[Ca^{2+}-Ge^{4+}]$ for $[Lu^{3+}-Al^{3+}]$ was used to change the crystal lattice environment around the Eu^{2+} ion in a possible wider range. Under an excitation wavelength of 365 nm, the normalized emission spectrum presented an obvious red-shift phenomenon with increasing concentration of $[Ca^{2+}-Ge^{4+}]$, as shown in Figure 7a. The maximum peak in the PL spectra moved from 463 nm
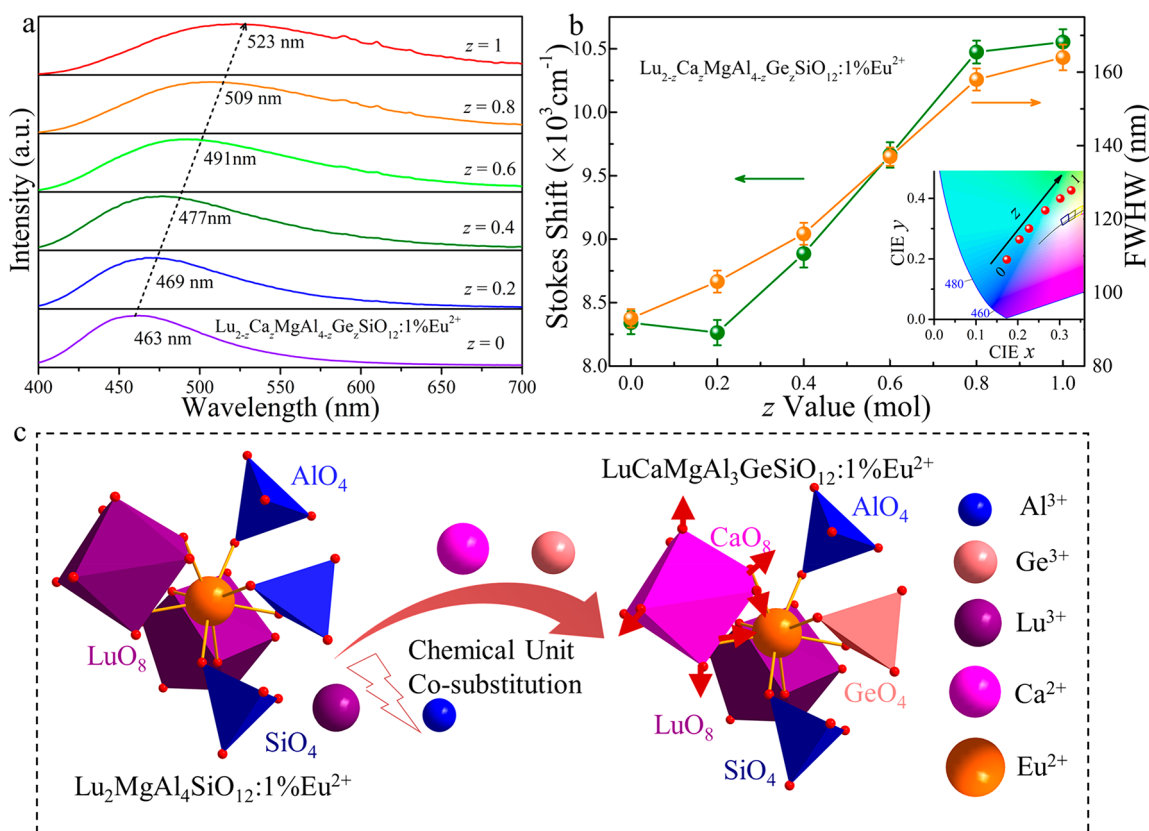
Figure 7. (a) PL spectra of the $Lu_{2-z}Ca_zMgAl_{4-z}Ge_zSiO_{12}$:1%$Eu^{2+}$ phosphors monitored at 365 nm. (b) Stokes shift and fwhm values of the $Lu_{2-z}Ca_zMgAl_{4-z}Ge_zSiO_{12}$:1%$Eu^{2+}$ phosphors. The inset show the CIE chromaticity coordinates. (c) Shrinkage mechanism of the EuO_8 polyhedron with $Ca^{2+}-Ge^{4+}$ substituting for $Lu^{3+}-Al^{3+}$ in $Lu_{2-z}Ca_zMgAl_{4-z}Ge_zSiO_{12}$:1%$Eu^{2+}$.

for $z = 0$ to 523 nm for $z = 1$, which may be caused by improvement of the crystal-field-splitting energy. Besides, the CIE coordinates of the $Lu_{2-z}Ca_zMgAl_{4-z}Ge_zSiO_{12}$:1%$Eu^{2+}$ phosphors gradually shifted from the blue region with the coordinate of (0.174, 0.198) to the green region of (0.328, 0.427) through an increase in the $[Ca^{2+}\text{-}Ge^{4+}]$ doping content. However, the addition of $[Ca^{2+}-Ge^{4+}]$ in the $Lu_2MgAl_4SiO_{12}$:1%Eu^{2+} sample would also do great damage to the symmetry of the Eu^{2+} local coordinated environment, leading to the emergence of a Eu^{3+} emission in $z = 0.6-1$. Overall, Figure 7b shows an increase of the Stokes shift and fwhm value of the emission spectra with enhancement of the z value due to contraction of the EuO_8 polyhedron. Furthermore, the local structure evolution model through replacement of the $[LuO_8]$ polyhedron and $[AlO_4]$ tetrahedron by the larger $[CaO_8]$ and similar $[GeO_4]$ is presented in Figure 7c, and a typical distortion can be observed because of breaking of the symmetry of the $[EuO_8]$ dodecahedron. Thus, the red-shift and broadening emission band were mainly influenced by enhancement of the polyhedral distortion.

CONCLUSION

Eu^{2+}-doped garnet-type phosphors were designed based on multiple substitution strategies to modify the chemical compositions and further tune the PL. The $Lu_2MgAl_4SiO_{12}$:1%Eu^{2+} phosphor exhibited blue emission with an asymmetric emission band under 365 nm UV-light excitation, which was ascribed to the two-site occupation of Eu^{2+} at Lu and Mg crystallographic sites, and, accordingly, the emission peak positions moved about 15 nm to longer

wavelengths with increasing Eu^{2+} content. Moreover, the red-shift behavior from 463 to 503 nm along with the broadening emission band can be realized via replacement of Mg^{2+} with Ca^{2+} in the $Lu_2MgAl_4SiO_{12}$:1%Eu^{2+} system. In the meantime, chemical unit cosubstitution of $[Ca^{2+}-Ge^{4+}]$ for $[Lu^{3+}-Al^{3+}]$ has been successfully adopted to adjust the maximum peak of the PL from 463 to 523 nm and broaden the fwhm value of the emission spectra. These changes in the PL spectra were caused by enhancement of the polyhedral distortion in the EuO_8 polyhedron with an increase in the amounts of Ca or Ca and Ge. This work demonstrated that it is efficient to design novel Eu^{2+}-doped garnet-type phosphors based on control of the chemical composition of the hosts via cation substitution and the chemical unit cosubstitution method to realize color-tunable emission.

ASSOCIATED CONTENT

Ⓢ Supporting Information

The Supporting Information is available free of charge at https://pubs.acs.org/doi/10.1021/acs.inorgchem.9b03142.

Tables S1−S4 and Figure S1 (PDF)

AUTHOR INFORMATION

Corresponding Author

*Email: xiazg@scut.edu.cn.

ORCID Ⓘ

Jing Zhao: 0000-0002-8000-5973

Hendrik C. Swart: 0000-0001-5233-0130

Zhiguo Xia: 0000-0002-9670-3223

■ **REFERENCES**

(1) Li, G. G.; Tian, Y.; Zhao, Y.; Lin, J. Recent progress in luminescence tuning of Ce^{3+} and Eu^{2+}-activated phosphors for pc-WLEDs. *Chem. Soc. Rev.* **2015**, *44* (23), 8688−8713.

(2) Xia, Z. G.; Liu, Q. L. Progress in discovery and structural design of color conversion phosphors for LEDs. *Prog. Mater. Sci.* **2016**, *84*, 59−117.

(3) Qin, X.; Liu, X. W.; Huang, W.; Bettinelli, M.; Liu, X. G. Lanthanide-Activated Phosphors Based on 4f-5d Optical Transitions: Theoretical and Experimental Aspects. *Chem. Rev.* **2017**, *117*, 4488−4527.

(4) Im, W. B.; George, N.; Kurzman, J.; Brinkley, S.; Mikhailovsky, A.; Hu, J.; Chmelka, B. F.; DenBaars, S. P.; Seshadri, R. Efficient and color-tunable oxyfluoride solid solution phosphors for solid-state white lighting. *Adv. Mater.* **2011**, *23* (20), 2300−2305.

(5) Dai, P. P.; Li, C.; Zhang, X. T.; Xu, J.; Chen, X.; Wang, X. L.; Jia, Y.; Wang, X.; Liu, Y. C. A single Eu^{2+}-activated high-color-rendering oxychloride white-light phosphor for white-light-emitting diodes. *Light: Sci. Appl.* **2016**, *5* (2), e16024.

(6) Xia, Z.; Meijerink, A. Ce^{3+}-Doped garnet phosphors: composition modification, luminescence properties and applications. *Chem. Soc. Rev.* **2017**, *46* (1), 275−299.

(7) Xie, R.-J.; Hirosaki, N.; Mitomo, M.; Suehiro, T.; Xu, X.; Tanaka, H. Photoluminescence of Rare-Earth-Doped Ca-alpha-SiAlON Phosphors: Composition and Concentration Dependence. *J. Am. Ceram. Soc.* **2005**, *88* (10), 2883−2888.

(8) Zhang, M.; Wang, J.; Ding, W.; Zhang, Q.; Su, Q. Luminescence properties of $M_2MgSi_2O_7$:Eu^{2+} (M = Ca, Sr) phosphors and their effects on yellow and blue LEDs for solid-state lighting. *Opt. Mater.* **2007**, *30* (4), 571−578.

(9) Denault, K. A.; George, N. C.; Paden, S. R.; Brinkley, S.; Mikhailovsky, A. A.; Neuefeind, J.; DenBaars, S. P.; Seshadri, R. A green-yellow emitting oxyfluoride solid solution phosphor Sr_2Ba-$(AlO_4F)_{1−x}(SiO_5)_x$:Ce^{3+} for thermally stable, high color rendition solid state white lighting. *J. Mater. Chem.* **2012**, *22* (35), 18204−18213.

(10) Pust, P.; Weiler, V.; Hecht, C.; Tucks, A.; Wochnik, A. S.; Henss, A. K.; Wiechert, D.; Scheu, C.; Schmidt, P. J.; Schnick, W. Narrow-band red-emitting $Sr[LiAl_3N_4]$:Eu^{2+} as a next-generation LED-phosphor material. *Nat. Mater.* **2014**, *13* (9), 891−896.

(11) Wei, Y.; Gao, J.; Xing, G.; Li, G.; Dang, P.; Liang, S.; Huang, Y. S.; Lin, C. C.; Chan, T.-S.; Lin, J. Controllable Eu^{2+}-Doped Orthophosphate Blue-/Red-Emitting Phosphors: Charge Compensation and Lattice-Strain Control. *Inorg. Chem.* **2019**, *58* (9), 6376−6387.

(12) Zhou, Y. N.; Zhuang, W. D.; Hu, Y. S.; Liu, R. H.; Xu, H. B.; Chen, M. Y.; Liu, Y. H.; Li, Y. F.; Zheng, Y. L.; Chen, G. T. Cyan-Green Phosphor $Lu_2M(Al_4Si)O_{12}$:Ce^{3+} for High-Quality LED Lamp: Tunable Photoluminescence Properties and Enhanced Thermal Stability. *Inorg. Chem.* **2019**, *58* (2), 1492−1500.

(13) Shang, M.; Fan, J.; Lian, H.; Zhang, Y.; Geng, D.; Lin, J. A double substitution of Mg^{2+}-Si^{4+}/Ge^{4+} for $Al(1)^{3+}$-$Al(2)^{3+}$ in Ce^{3+}-doped garnet phosphor for white LEDs. *Inorg. Chem.* **2014**, *53* (14), 7748−7755.

(14) Chen, Y.; Feng, D.; Xu, S.; Zeng, S.; Wei, X. Synthesis and photoluminescence of Eu^{2+} doped $Lu_2CaMg_2Si_3O_{12}$ garnet phosphors. *Mater. Lett.* **2016**, *164*, 180−182.

(15) Zhang, X.; An, Z.; Dong, R.; Song, Y.; Zheng, K.; Sheng, Y.; Shi, Z.; Zou, H. Properties and Application of Single Eu^{2+}-Activated Color Tuning Phosphors. *ACS Sustainable Chem. Eng.* **2019**, *7* (12), 10724−10733.

(16) Berezovskaya, I. V.; Dotsenko, V. P.; Voloshinovskii, A. S.; Smola, S. S. Near infrared emission of Eu^{2+} ions in $Ca_3Sc_2Si_3O_{12}$. *Chem. Phys. Lett.* **2013**, *585*, 11−14.

(17) Wang, S. S.; Chen, W. T.; Li, Y.; Wang, J.; Sheu, H. S.; Liu, R. S. Neighboring-cation substitution tuning of photoluminescence by remote-controlled activator in phosphor lattice. *J. Am. Chem. Soc.* **2013**, *135* (34), 12504−12507.

(18) Li, G.; Lin, C. C.; Chen, W.-T.; Molokeev, M. S.; Atuchin, V. V.; Chiang, C.-Y.; Zhou, W.; Wang, C.-W.; Li, W.-H.; Sheu, H.-S.; Chan, T.-S.; Ma, C.; Liu, R.-S. Photoluminescence Tuning via Cation Substitution in Oxonitridosilicate Phosphors: DFT Calculations, Different Site Occupations, and Luminescence Mechanisms. *Chem. Mater.* **2014**, *26* (9), 2991−3001.

(19) Wang, L.; Xie, R. J.; Li, Y.; Wang, X.; Ma, C. G.; Luo, D.; Takeda, T.; Tsai, Y. T.; Liu, R. S.; Hirosaki, N. $Ca_{1−x}Li_xAl_{1−x}Si_{1+x}N_3$:$Eu^{2+}$ solid solutions as broadband, color-tunable and thermally robust red phosphors for superior color rendition white light-emitting diodes. *Light: Sci. Appl.* **2016**, *5* (10), e16155.

(20) Huang, C.-H.; Wu, P.-J.; Lee, J.-F.; Chen, T.-M. $(Ca,Mg,Sr)_9Y$-$(PO_4)_7$:Eu^{2+},Mn^{2+}: Phosphors for white-light near-UV LEDs through crystal field tuning and energy transfer. *J. Mater. Chem.* **2011**, *21* (28), 10489−10495.

(21) Liang, S.; Dang, P.; Li, G.; Wei, Y.; Wei, Y.; Lian, H.; Lin, J. New Insight for Luminescence Tuning Based on Interstitial sites Occupation of Eu^{2+} in $Sr_3Al_{2−x}SixO_{5−x}N_xCl_2$ (x = 0−0.4). *Adv. Opt. Mater.* **2018**, *6*, 1800940.

(22) Qiao, J.; Zhang, Z.; Zhao, J.; Xia, Z. Tuning of the Compositions and Multiple Activator Sites toward Single-Phased White Emission in $(Ca_{9−x}Sr_x)MgK(PO_4)_7$:$Eu^{2+}$ Phosphors for Solid-State Lighting. *Inorg. Chem.* **2019**, *58* (8), 5006−5012.

(23) Xia, Z.; Ma, C.; Molokeev, M. S.; Liu, Q.; Rickert, K.; Poeppelmeier, K. R. Chemical Unit Cosubstitution and Tuning of Photoluminescence in the $Ca_2(Al_{1−x}Mg_x)(Al_{1−x}Si_{1+x})O_7$:$Eu^{2+}$ Phosphor. *J. Am. Chem. Soc.* **2015**, *137* (39), 12494−12497.

(24) Prashantha, S. C.; Lakshminarasappa, B. N.; Nagabhushana, B. M. Photoluminescence and thermoluminescence studies of Mg_2SiO_4:Eu^{3+} nano phosphor. *J. Alloys Compd.* **2011**, *509* (42), 10185−10189.

(25) Ding, X.; Zhu, G.; Geng, W.; Mikami, M.; Wang, Y. Novel blue and green phosphors obtained from $K_2ZrSi_3O_9$:Eu^{2+} compounds with different charge compensation ions for LEDs under near-UV excitation. *J. Mater. Chem. C* **2015**, *3*, 6676−6685.

(26) Xiao, W.; Zhang, X.; Hao, Z.; Pan, G. H.; Luo, Y.; Zhang, L.; Zhang, J. Blue-emitting $K_2Al_2B_2O_7$:Eu^{2+} phosphor with high thermal stability and high color purity for near-UV-pumped white light-emitting diodes. *Inorg. Chem.* **2015**, *54* (7), 3189−3195.

(27) Leng, Z.; Li, R.; Li, L.; Xue, D.; Zhang, D.; Li, G.; Chen, X.; Zhang, Y. Preferential Neighboring Substitution-Triggered Full Visible Spectrum Emission in Single-Phased $Ca_{10.5−x}Mg_x(PO_4)_7$:Eu^{2+} Phosphors for High Color-Rendering White LEDs. *ACS Appl. Mater. Interfaces* **2018**, *10* (39), 33322−33334.

(28) Shang, M.; Liang, S.; Qu, N.; Lian, H.; Lin, J. Influence of Anion/Cation Substitution ($Sr^{2+} \rightarrow Ba^{2+}$, $Al^{3+} \rightarrow Si^{4+}$, $N^{3−} \rightarrow O^{2−}$) on Phase Transformation and Luminescence Properties of $Ba_3Si_6O_{15}$:Eu^{2+} Phosphors. *Chem. Mater.* **2017**, *29* (4), 1813−1829.

(29) Wang, Y.; Ding, J.; Wang, Y. $Ca_{2−x}Y_{1+x}Zr_{2−x}Al_{3+x}O_{12}$:$Ce^{3+}$: Solid Solution Design toward the Green Emission Garnet Structure Phosphor for Near-UV LEDs and Their Luminescence Properties. *J. Phys. Chem. C* **2017**, *121* (48), 27018−27028.

(30) Denault, K. A.; Brgoch, J.; Gaultois, M. W.; Mikhailovsky, A.; Petry, R.; Winkler, H.; DenBaars, S. P.; Seshadri, R. Consequences of Optimal Bond Valence on Structural Rigidity and Improved Luminescence Properties in $Sr_xBa_{2−x}SiO_4$:Eu^{2+} Orthosilicate Phosphors. *Chem. Mater.* **2014**, *26* (7), 2275−2282.

(31) Baur, W. H. The geometry of polyhedral distortions. Predictive relationships for the phosphate group. *Acta Crystallogr., Sect. B: Struct. Crystallogr. Cryst. Chem.* **1974**, *30* (5), 1195−1215.